Coverage-dependent dipole coupling for carbon monoxide adsorbed at ordered platinum(111)-aqueous interfaces: Structural and electrochemical implications

Si-Chung Chang and Michael J. Weaver
Department of Chemistry, Purdue University, West Lafayette, Indiana 47907

(Received 21 August 1989; accepted 18 December 1989)

Surface infrared spectra in the terminal C–O stretching region are reported for various $^{12}CO/^{13}CO$ mixtures adsorbed on an ordered Pt(111) electrode in 0.1 M $HClO_4$ as a function of CO coverage θ ($0.05 \lesssim \theta \lesssim 0.6$) and electrode potential E. Contributions to the coverage-induced shift in the C–O stretching frequency ν^t_{CO} arising from dynamic dipole–dipole coupling $\Delta\nu_D$, and from static dipole and "chemical" effects $\Delta\nu_C$, are obtained from the mixed isotope spectra. Similar to the corresponding ultrahigh vacuum (UHV) system, the former provides the largest contribution, $\Delta\nu_D$ being 30–35 cm^{-1} for saturated CO layers ($\theta \approx 0.6$). Substantial differences in the ν^t_{CO}-θ (and $\Delta\nu_D$-θ) dependencies were observed for CO adlayers formed by dosing from suitably low solution concentrations ($\sim 2\times10^{-5}$ M), and from saturated irreversibly adsorbed layers by means of partial electrooxidative stripping. Using the latter "stripping" procedure, only small ($\lesssim 5$ cm^{-1}) decreases in ν^t_{CO} and $\Delta\nu_D$ were observed as θ is decreased over the range $0.1 \lesssim \theta < 0.6$, whereas the former "dosing" procedure yielded substantially larger ν^t_{CO}-θ and $\Delta\nu_D$-θ dependencies, especially in the presence of coadsorbed hydrogen (at -0.25 V vs SCE) rather than coadsorbed water (at 0.1 V). These behavioral differences are interpreted in terms of coverage-dependent CO island formation. For electrooxidative stripping conditions, extensive island formation survives to low CO coverages, providing direct evidence that CO electrooxidation occurs via nucleation and growth at the island edges. For dosing conditions, smaller and more coverage-dependent CO patches are apparently obtained in the presence of coadsorbed hydrogen. These undergo slightly more facile electrooxidation than the CO islands formed at intermediate coverages by prior stripping. The coverage-dependent frequencies and intensities of the bridging CO form ($\nu^b_{CO} \approx 1800$–1850 cm^{-1}) vs the terminal CO form ($\nu^t_{CO} \approx 2020$–2075 cm^{-1}) are also examined in comparison with corresponding data for related UHV systems. In contrast to Pt(111)/CO in UHV, the bridging site is occupied even at low dosed coverages ($\theta \gtrsim 0.05$): this is also suggestive of the presence of CO islands having high local coverages. Similarities are noted with vibrational spectra obtained for Pt(111)/CO with coadsorbed water and hydrogen in UHV.

INTRODUCTION

The use of vibrational spectroscopic probes, especially infrared reflection–absorption spectroscopy (IRRAS) and electron energy loss spectroscopy (EELS), to characterize small molecule adsorbates at ordered monocrystalline surfaces in ultrahigh vacuum (UHV) has yielded a wealth of structural information.[1] The recent advent of IRRAS as applied to metal–solution interfaces,[2] coupled with the development of reliable means of preparing well-ordered single-crystal surfaces for *in situ* electrochemical purposes,[3,4] is providing important new opportunities for the corresponding structural characterization of such systems. Apart from the rich structural and dynamical information that can be obtained for such well-defined electrochemical systems in this manner, comparisons between corresponding vibrational spectra obtained for the same adsorbates in UHV and electrochemical environments can yield insight into the influence of the solution phase for the latter case.

The obvious adsorbate from this standpoint to select initially is carbon monoxide in view of the extensive characterization afforded this species in UHV, and the well-known sensitivity of the vibrational spectra of adsorbed CO to surface structure.[1] An additional importance of CO in electrochemical systems arises from its role in inhibiting the electrooxidation of organic molecules,[5] being commonly formed by dissociative reactant chemisorption in aqueous media.[6] Not surprisingly, then, most electrochemical IRRAS studies reported so far involving single-crystal surfaces concern adsorbed CO on low-index platinum faces, formed either from solution CO[7–9] or from small organic molecules.[10,11] Related recent studies have examined CO on Rh(111)[11(b),12(a)] and Rh(100).[12(b)]

An issue of central significance concerns the dependence of the CO layer structure upon the fractional adsorbate coverage θ. The Pt(111)/CO system in UHV has been widely studied in this regard, utilizing in particular structural information obtained from low energy electron diffraction (LEED) in conjunction with IRRAS.[13,14] We recently examined in some detail the dependencies upon θ and the electrode potential E of the frequency and intensity of the C–O stretching mode ν_{CO} for CO on Pt(111) in an acidic aqueous environment.[9(a)] In some respects, the coverage-dependent ν_{CO} bands for the terminal and bridging CO (ap-

 0021-9606/90/074582-13$03.00

pearing at ~2020–2075 and 1800–1850 cm^{-1}, respectively) exhibit behavior comparable to that in the corresponding UHV environment. Thus the intensity of the latter band maximizes for coverages below saturation, similar to IRRAS results in UHV,[15] suggesting that there is a vestige of the $c(4\times2)$ overlayer structure in the electrochemical environment, featuring occupancy of CO molecules into twofold bridge as well as terminal sites[14] (*vide infra*). In addition, the frequencies of the terminal C–O stretch ν_{CO}^{t} on Pt(111), and on Pt(100) and Pt(110), in the electrochemical systems are similar to those in UHV when account is taken of the different electrostatic potentials that typify these environments.[9(b)–9(d)]

A tactic that has proved valuable for characterizing adsorbate interactions in UHV involves obtaining coverage-dependent infrared spectra for various proportions of isotopic mixtures, such as $^{12}CO/^{13}CO$.[16] The procedure enables alterations in vibrational frequencies brought about by adsorbate–adsorbate interactions $\Delta\nu$ to be separated into components associated with dynamic dipole–dipole coupling $\Delta\nu_D$ and "static" dipole and chemical contributions $\Delta\nu_C$.[16] This is because the former component will be diminished considerably, yet the latter contribution unaffected, by diluting an adsorbate layer at a given coverage with isotopically substituted adsorbate having a sufficiently different singleton frequency.

Such tactics would appear to provide an appealing means of exploring the effects of the double-layer environment on the coverage-dependent structure of electrochemical adsorbates. So far, however, only isolated studies of adsorbate dipole coupling at electrochemical interfaces have been reported, and these refer to polycrystalline metal surfaces.[17,18] Described herein is an examination of dipole coupling for terminal adsorbed CO on ordered Pt(111) in aqueous 0.1 M $HClO_4$, employing coverage-dependent ν_{CO} infrared spectra for $^{12}CO/^{13}CO$ mixtures. Corresponding information for this system in UHV is available from a recent study at essentially the same temperature, 300 K,[19] as well as for the lower temperatures more commonly used for such studies.[13(a)] The results uncover interesting differences in the coverage-dependent dipole coupling at electrode potentials where coadsorbed hydrogen is present rather than water. Marked adsorbate structural differences, specifically in the nature and extent of CO "island" formation, are also deduced in this manner for layers formed by electrooxidative removal from higher coverages rather than by direct dosage with suitably low concentrations of solution CO.

EXPERIMENTAL SECTION

Details of the electrochemical IRRAS measurements are largely as provided in Refs. 20 and 21. The infrared spectrometer was an IBM (Bruker) IR-98-4A vacuum Fourier transform instrument, with a Globar light source and either an InSb or MCT detector (Infrared Associates). The former detector was chosen so to yield optimal signal to noise for the terminal ν_{CO} band. Its use essentially precludes detection of the lower-frequency bridge-bound feature, located at or below the detector cutoff frequency at ~1830 cm^{-1}. The MCT detector was therefore utilized when both the bridging and terminal bands were desired to be observed. The spectral resolution was usually ± 4 cm^{-1}, although greater resolution (± 2 cm^{-1}) was employed when accurate bandwidth information was required. A modification from earlier studies is the present use of a CaF_2 prism, cut at 60° to the surface normal, as the window on the electrochemical IRRAS cell in place of a flat CaF_2 plate. Since the IR beam is also incident on the window at an angle of ~60°, the prism arrangement minimizes the extent of refraction at the air–CaF_2 interface and hence maximizes the angle of incidence at the metal–aqueous interface as is desirable for surface infrared studies.[22,23] (Typically, the effective absorbances for adsorbed species are observed to be ~three-fold larger when using the prism rather than the flat window arrangement.)

The Pt(111) crystal (9 mm diameter, 4 mm thick) was purchased from the Material Preparation Facility at Cornell University. It was oriented within $\pm$ 1°, as verified by x-ray diffraction. Procedural details, including surface preparation, are described in Ref. 9(a). The ^{12}CO (99.8%) was obtained from Matheson, and ^{13}CO (99%) from Aldrich. The preparation of the desired $^{12}CO/^{13}CO$ mixtures for dosage into the IRRAS cell was as follows. A flask containing 100 ml of nitrogen-purged 0.1 M $HClO_4$ was fed into the glass container containing the ^{13}CO via a vacuum stopcock connection. After shaking for ~30 min, the solution was fed back into the flask and sealed separately. Small (5 ml) aliquots were pipetted into vials prior to use. A series of vials containing ^{12}CO-saturated 0.1 M $HClO_4$ were also prepared by CO purging. Appropriate mixtures of these 0.1 M $HClO_4$ solutions were then prepared immediately prior to pipetting into the IRRAS cell so to yield the desired $^{12}CO/^{13}CO$ concentrations. The IRRAS cell initially contained nitrogen-purged 0.1 M $HClO_4$.

A variety of CO dosing conditions were employed (*vide infra*). Most commonly, however, the Pt(111) electrode was pulled back from the CaF_2 optical window so to expose the surface to the bulk solution for a predetermined time before reforming the electrochemical thin layer by pushing the electrode back up to the window. The precise coverages of ^{13}CO and ^{12}CO present on the electrode surface were determined from the corresponding infrared band intensities for the CO_2 formed by CO electrooxidation, as is outlined below. The thin-layer thickness, ~5 μm, is sufficiently small so that for the dilute CO solutions typically used, $\lesssim 2\times10^{-5}$ M, the contribution to the amount of CO_2 formed from thin-layer solution, rather than adsorbed, CO was minor and usually negligible. When dosing with higher CO solution concentrations (such as near-saturated conditions, ~1 mM, prepared by ^{12}CO purging), subsequent nitrogen purging was undertaken for 10 minutes so to remove the solution CO.

Electrode potentials are quoted vs the saturated calomel electrode (SCE), and all measurements were performed at room temperature, 23 $\pm$ 1 °C.

RESULTS

The basic strategy pursued here is to obtain ν_{CO} infrared spectra at the Pt(111)–aqueous 0.1 M $HClO_4$ interface for

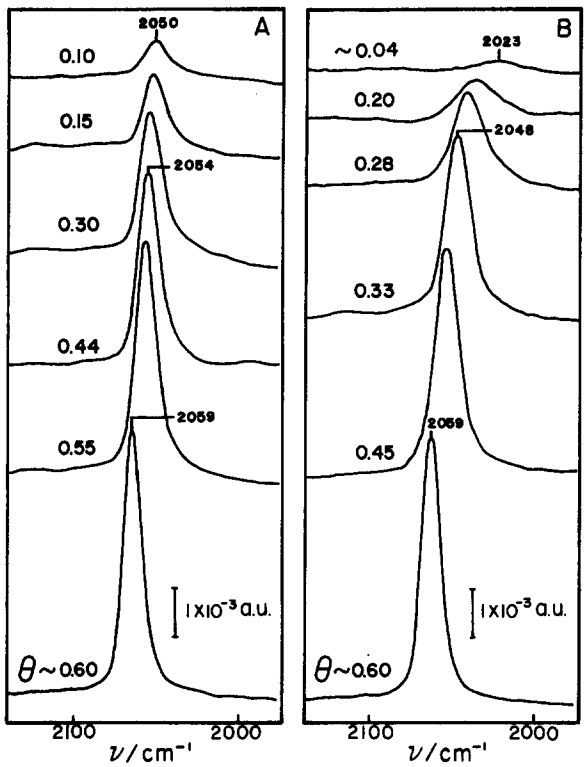

FIG. 1. Infrared absorbance spectra in terminal C–O stretching region for irreversibly adsorbed CO layers on ordered Pt(111) in 0.1 M $HClO_4$ at -0.25 V vs SCE with coverage values (θ) as indicated. Spectra in (A) and (B) obtained by progressive electrooxidative stripping from a saturated ($\theta \approx 0.6$) layer and by dosing for variable times from dilute ($\sim 2\times10^{-5}$ M) CO solutions, respectively. Each spectrum was acquired by means of 30 interferometer scans, and subtracting another set obtained subsequently at 0.5 V after CO electrooxidation was complete. Coverage values obtained from faradaic charge for voltammetric oxidation, and from absorbance of product solution CO_2 band at 2343 cm^{-1}. See the text for further details.

sequencies of CO coverages θ with various $^{12}CO/^{13}CO$ isotopic ratios. Data were obtained at two different electrode potentials, -0.25 V and $+0.1$ V vs SCE. These potentials were chosen so to correspond to the so-called "hydrogen" and "double-layer" regions, where the primary coadsorbed species are atomic hydrogen and water, respectively. Figures 1(A) and 1(B) contain representative infrared absorbance spectra at -0.25 V in the 1950–2150 cm^{-1} region for pure ^{12}CO layers at the various coverages indicated. The left-hand set [Fig. 1(A)] were obtained by starting with a saturated, irreversibly adsorbed, CO layer formed by bubbling in ^{12}CO for a few minutes, and then purging with nitrogen before forming the thin layer. The saturation coverage, $\theta = 0.6_2$, similar to that observed for the UHV system,[24] is determined from the faradaic charge required to voltammetrically oxidize the CO adlayer to CO_2.[9] (As usual, θ refers to the ratio of adsorbed CO molecules to platinum surface atoms.) The bottom spectrum in Fig. 1(A) refers to this coverage, whereas the upward sequence of spectra shown were obtained for progressively diminishing coverages, as indicated.

The procedure used to obtain these spectra entailed acquiring sets of 30 interferometer scans at -0.25 V, stepping the potential to 0.5 V for ~ 2 s between each set so as to electrooxidize a fraction of the adsorbed CO each time. Subtracted from each set is a corresponding spectrum obtained after the electrooxidation is complete, so to eliminate spectral interferences from the solvent, etc. [cf. Ref. 21(a)]. The intermediate coverages indicated were obtained from the absorbance of the solution CO_2 band at 2343 cm^{-1}, also appearing in these potential-difference spectra.[21] (Given the high intensity of the 2343 cm^{-1} feature,[21] this procedure provides an accurate as well as convenient means of monitoring the CO coverage[25]; at least the *relative* θ values are accurate to $\sim 5\%$.)

The right-hand set of spectra [Fig. 1(B)] were obtained instead by exposing the Pt(111) surface at -0.25 V to a lower CO solution concentration ($\sim 2\times10^{-5}$ M) for varying periods. Attainment of a saturated layer, $\theta = 0.6$, required about 10 min; lower coverages were obtained by employing shorter dosing times. Each spectrum shown was obtained by acquiring 50 interferometer scans at -0.25 V and subsequently at 0.5 V following complete CO electrooxidation, the latter set being subtracted from the former. As before, the CO coverage was obtained from the absorbance of the corresponding 2343 cm^{-1} product band also appearing in these spectra. Signal-to-noise considerations set a detection limit for stripped and dosed layers under these conditions of around $\theta \approx 0.02$ and 0.05, respectively.

Comparison of Figs. 1(A) and 1(B) reveals marked differences in the form of the coverage-dependent terminal ν_{CO} band under such CO stripping and dosing conditions. The peak frequency ν'_{CO} in the former case decreases by only 10 cm^{-1}, from about 2060 to 2050 cm^{-1}, over the θ range 0.6 to 0.1, and the bandwidth remains largely unchanged. In contrast, greater decreases in ν'_{CO}, to 2025 cm^{-1} at $\theta = 0.1$, are observed in the latter case along with marked increases in the bandwidth [Fig. 1(B)]. Similar ν'_{CO}-θ behavior was also obtained under stripping conditions if the partial electrooxidation was performed with the electrode retracted from the optical window rather than within the thin-layer configuration. The ν'_{CO} values were also maintained at a given coverage formed by either stripping or dosing for at least 30 min, indicating that the distinct adlayer structures thus formed are not interconverted on this timescale. Essentially equivalent results were obtained under these conditions by using ^{13}CO in place of ^{12}CO, except that the ν_{CO} frequencies are downshifted uniformly by 45–50 cm^{-1} as expected from the carbon mass change. The observed $^{13}CO/^{12}CO$ ν'_{CO} ratio, 0.977, is very close to that observed for the UHV Pt(111)/CO system,[26] and to the ratio expected on the basis of the reduced masses of isolated CO molecules.

Figures 2(A) and 2(B) contain corresponding coverage-dependent spectra, i.e., for CO stripping and dosing conditions, obtained for approximately 1:1 $^{12}CO/^{13}CO$ mixtures. The precise composition of the isotopic mixture (46% ^{12}CO) was deduced from the intensities of the 2343 and 2275 cm^{-1} product bands, corresponding to $^{12}CO_2$ and $^{13}CO_2$, corrected for the slight anticipated difference in absorptivity resulting from isotopic substitution.[27] The hallmarks of strong dipole–dipole coupling are seen for $\theta \sim 0.6$, in that the ^{12}CO ν_{CO} frequency is downshifted substantially (by 20 cm^{-1}) and there is considerable "intensity transfer" to the

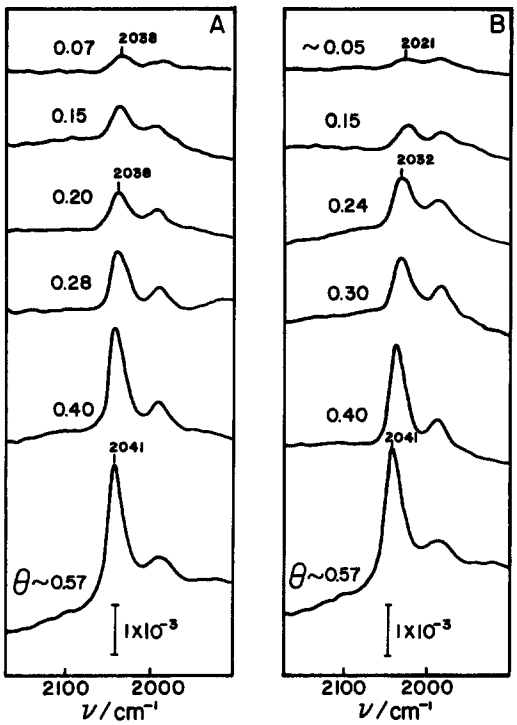

FIG. 2. As in Fig. 1, but for $^{12}CO/^{13}CO$ adsorbate mixture containing 46% ^{12}CO. Precise isotopic composition determined from relative intensities of $^{12}CO_2$ $^{13}CO_2$ product bands at 2343 and 2275 cm^{-1}, respectively (see the text).

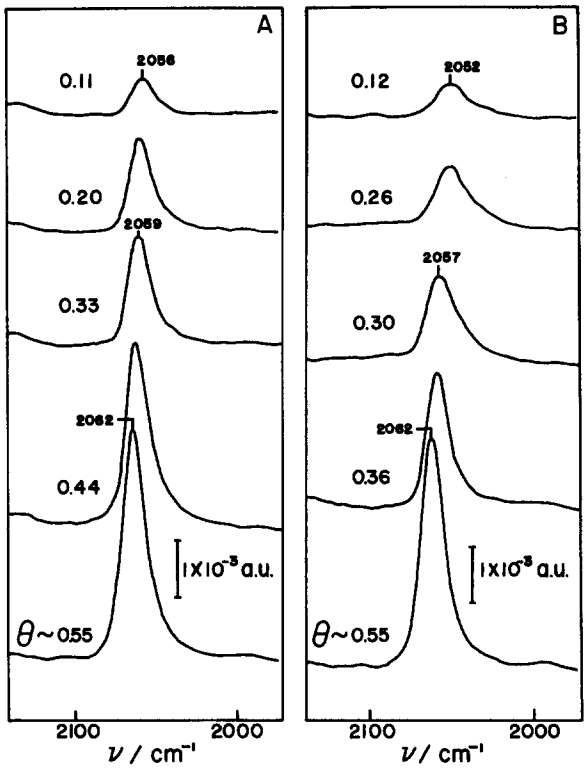

FIG. 3. As in Fig. 1, but for adsorption at 0.1 V vs SCE.

higher-frequency band component. Both these features are closely similar to those observed for saturation coverages in the corresponding UHV Pt(111)/CO system at 300 K.[19,26] Significant differences are again seen for lower θ values under CO stripping vs dosing conditions. In the former case [Fig. 2(A)], the extent of dipole coupling seen for $\theta \sim 0.6$ is largely maintained down to low coverages, as gleaned most readily from the survival of extensive intensity transfer under these conditions. In the latter circumstances [Fig. 2(B)], however, the degree of dipole coupling diminishes to a greater extent towards lower coverages, as seen from the relative intensities of the band partners and from the smaller downshifts of the ^{12}CO ν_{CO} frequency under these conditions.

Figures 3(A) and 3(B) show coverage-dependent sets of ν_{CO} spectra for pure ^{12}CO obtained under stripping and dosing conditions as in Figs. 1(A) and 1(B), but for an adsorption potential of 0.1 V. Qualitatively similar features are observed as for adsorption at -0.25 V, in that CO dosing yields ν_{CO} bands which decrease in frequency to a greater extent than those obtained by electrooxidatively stripping the CO adlayer. However, the spectral differences resulting from these two adsorption conditions are smaller than observed at -0.25 V. Similar trends are also reflected in the corresponding spectra for $^{12}CO/^{13}CO$ mixtures.

Plots of the ν_{CO} bandwidth (*vide supra*), as reflected in the full width at half-maximum $\Delta\nu_{1/2}$, as a function of coverage are shown in Fig. 4 for adsorption at 0.1 V (triangles) as well as at -0.25 V (circles). Results obtained for stripping and dosing conditions are denoted by filled and open symbols, respectively. The former condition yields $\Delta\nu_{1/2}$ values (14–15 cm^{-1}) that are similar at 0.1 V and -0.25 V and essentially independent of θ. As already noted, the latter condition yields $\Delta\nu_{1/2}$ values at -0.25 V that increase substantially, from 15 to $\sim 30\,cm^{-1}$, as θ decreases. While qualitatively the same effect is observed at 0.1 V, the increase in $\Delta\nu_{1/2}$ (to $\sim 20\,cm^{-1}$) towards low θ is less pronounced than at -0.25 V (Fig. 4).

While the terminal ν_{CO} feature is of central concern

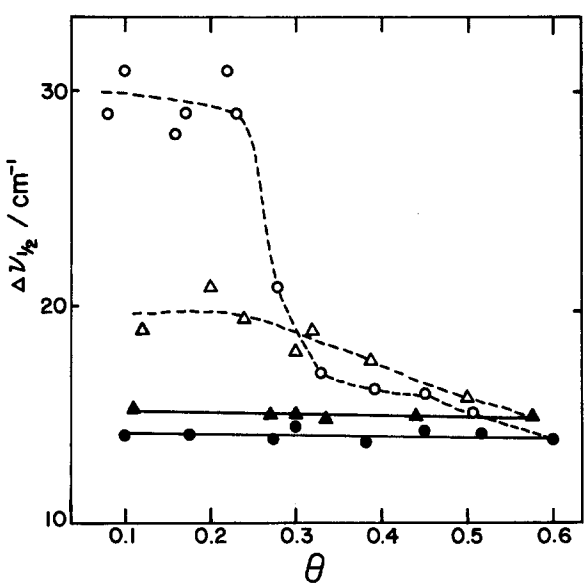

FIG. 4. The ν_{CO} bandwidth (i.e., full width at half maximum), $\Delta\nu_{1/2}$, vs CO coverage θ on Pt(111) for "dosing" (open symbols) and "electrooxidative stripping" conditions (filled symbols) at -0.25 V (circles) and 0.1 V (triangles).

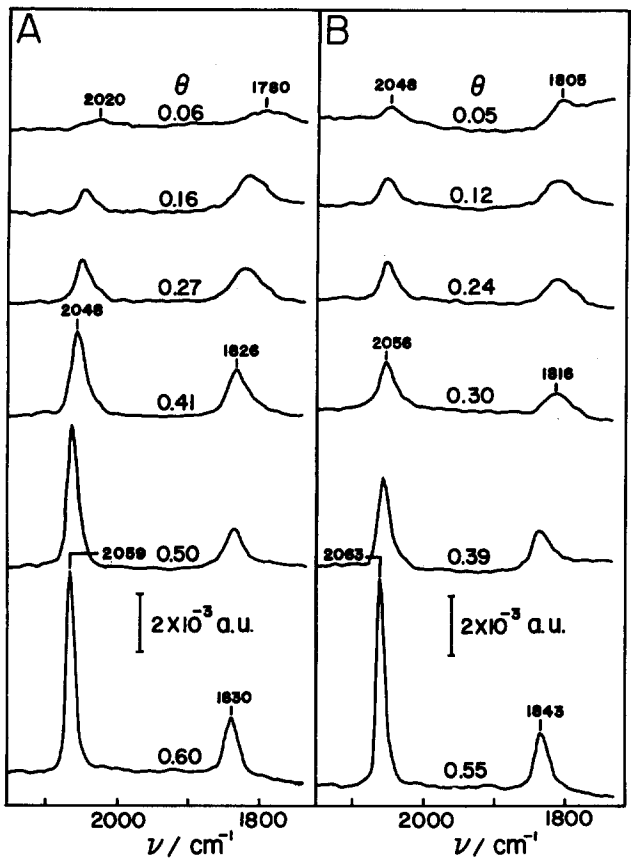

FIG. 5. Infrared absorbance spectra in 1750–2150 cm^{-1} region for dosed CO layers at coverages indicated on ordered Pt(111) in 0.1 M $HClO_4$ at (A) -0.25 V and (B) 0.1 V. Spectra obtained as in Fig. 1, but using 150 interferometer scans since MCT rather than InSb detector was employed.

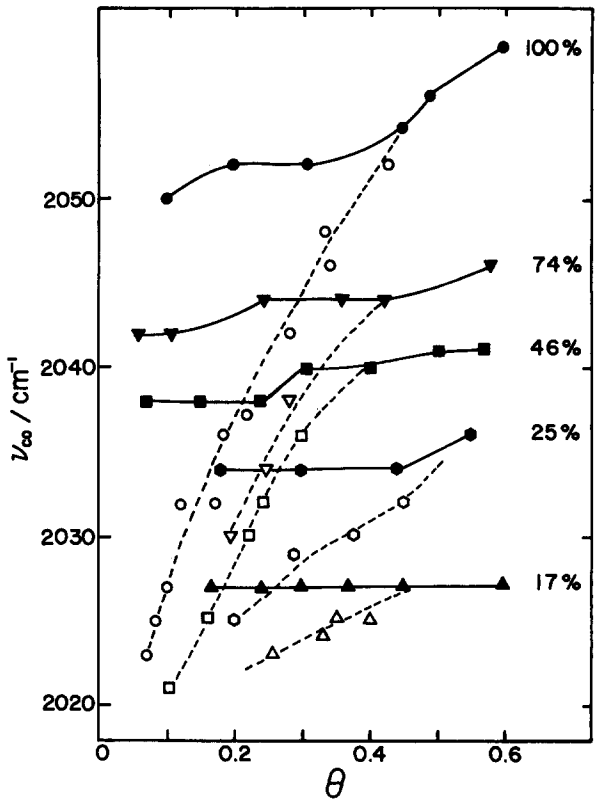

FIG. 6. Peak frequencies of higher-energy (^{12}CO) ν_{CO} band component for various $^{12}CO/^{13}CO$ mixtures vs total CO coverage θ on Pt(111) at -0.25 V for electrooxidative stripping (filled symbols, solid traces) and dosing conditions (open symbols, dashed traces). Percentage ^{12}CO present in each adsorbate isotopic mixture as indicated.

here, the properties of the bridging ν_{CO} band are also of interest, especially since comparison of these features sheds light on the coverage-dependent site occupancy. Figures 5(A) and 5(B) show sets of spectra for layers dosed to various coverages at -0.25 and 0.1 V, respectively, over the frequency range 1750–2150 cm^{-1} so to encompass the bridging as well as terminal bands. Similar θ-dependent behavior is seen at both potentials. While the latter band is substantially more intense at high coverages, the integrated absorbance of the bridging feature is relatively invariant with coverage so that for $\theta \lesssim 0.25$ it is more intense than the terminal band. The coverage dependence of the bridging ν_{CO} frequency ν^b_{CO}, is comparable to that for ν^t_{CO}. In addition, the bandwidth of the bridging ν_{CO} band increases with decreasing θ in a similar fashion to the terminal feature (Fig. 5). Under electrooxidative stripping conditions, in contrast, the relative intensity of the bridging feature remains markedly smaller than the terminal band even at low coverages, and neither ν^b_{CO} nor $\Delta\nu_{1/2}$ are altered greatly under these conditions [cf. Fig. 2(B) of Ref. 9(a)]. Interestingly, the bridging ν_{CO} band is virtually absent for saturated adlayers in the presence of solution CO, consistent with corresponding high-coverage UHV data where "compression structures" are formed.[13(a),15] The bridging ν_{CO} feature appears, however, upon initiating the layer electrooxidation.

Of central interest here is the coverage-dependent extent of dipole–dipole coupling for the terminal ν_{CO} band. Sequences of terminal ν_{CO} spectra, for CO coverages over the range $\sim$0.05–0.6 and for wide variations of the $^{12}CO/^{13}CO$ concentration ratio, were obtained for both stripping and dosing conditions. The resulting plots of the ^{12}C ν_{CO} frequencies vs θ for a series of $^{12}CO/^{13}CO$ mixtures (expressed as percentage ^{12}CO) for adsorption at -0.25 and 0.1 V are shown in Figs. 6 and 7, respectively. The filled and open symbols refer to CO stripping and dosing conditions, respectively. As expected, comparable results were also obtained by employing the low-frequency (^{13}CO) band component, but their reliability is impaired by the lower intensity of the ^{13}CO relative to the ^{12}CO band component in the isotopic mixtures. The differences between ν^t_{CO}–θ dependencies obtained under stripping and dosing conditions, evident for $\theta \lesssim 0.45$ and especially for adsorption at -0.25 V, are seen graphically in these figures. Experiments were also performed by dosing at -0.25 V to form a series of intermediate CO coverages, and examining the ν^t_{CO}–θ dependence for subsequent electrooxidative stripping. Interestingly, for $\theta < 0.4$ the ν^t_{CO}–θ curves extracted in this manner exhibited markedly greater downshifts in ν^t_{CO} with decreasing θ than are obtained by stripping from higher coverages, resembling more closely the corresponding plots obtained under purely dosing conditions.

The data in Figs. 6 and 7 were utilized in the conventional manner[16] to separate the dynamic dipole coupling ($\Delta\nu_D$)

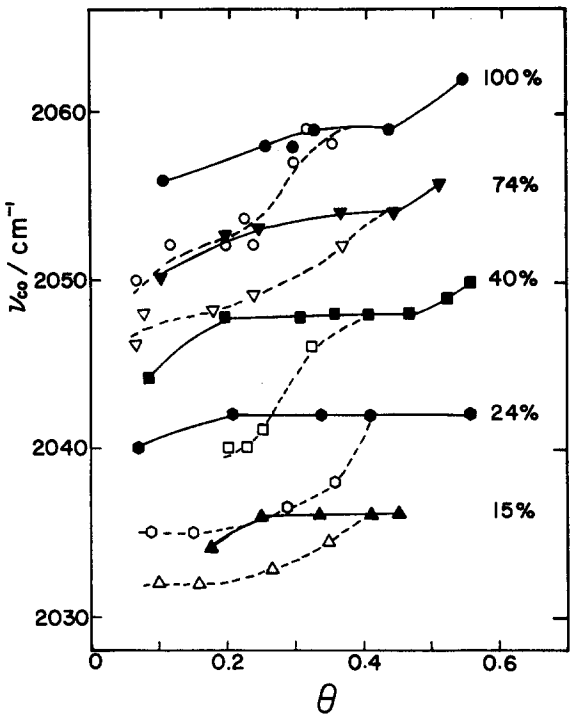

FIG. 7. As Fig. 6, but for adsorption at 0.1 V.

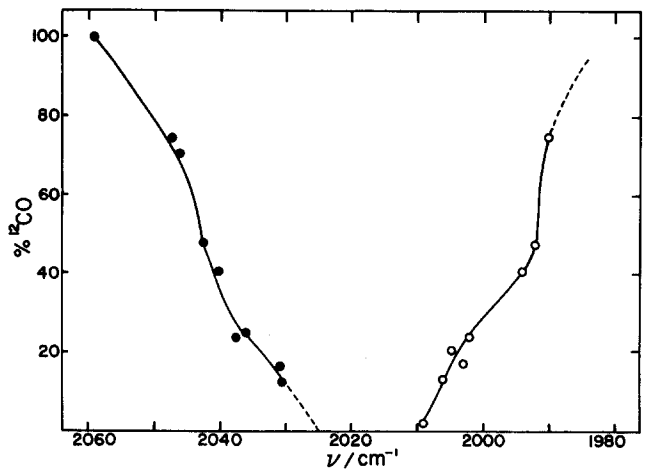

FIG. 8. Peak frequencies of higher-energy (^{12}CO) and lower-energy (^{13}CO) ν_{CO} band components (filled and open circles, respectively) plotted for various percentages of ^{12}CO present in an adsorbed ^{12}CO/^{13}CO mixture at a total CO coverage of 0.6 on Pt(111) at -0.25 V.

and "static" dipole and chemical contributions ($\Delta\nu_C$) to the overall coverage-dependent frequency shift $\Delta\nu$ as follows. The former quantity $\Delta\nu_D$ was determined as a function of θ from the difference between the measured ν_{CO} frequency for the pure ^{12}CO layer and that for the same coverage but in the dilution limit for ^{12}CO/^{13}CO mixtures, where $\%^{12}\text{CO}\rightarrow 0$, i.e.,

$$\Delta\nu_D(\theta) = \nu_{CO}(\theta) - \nu_{CO}(\theta,\text{dl}) \,. \quad (1)$$

The latter quantity, $\nu_{CO}(\theta,\text{dl})$, was extracted from the intercept of plots of the frequency of the ^{12}CO band partner against $\%^{12}$CO for each coverage. [Equation (1) follows from the virtual elimination of dynamic dipole coupling in the isotopic dilution limit, achieved in view of the differing ν_{CO} frequencies for ^{12}CO and ^{13}CO.[16]] The corresponding $\Delta\nu_C$ values were determined from

$$\Delta\nu_C(\theta) = \nu_{CO}(\theta,\text{dl}) - \nu_{CO}(\theta\rightarrow 0) \,, \quad (2)$$

where $\nu_{CO}(\theta\rightarrow 0)$ is the "singleton" frequency for vanishingly small coverages. This latter quantity was determined most reliably by extrapolating plots of the ν_{CO} frequency for the ^{12}CO band partner in relatively dilute ^{12}CO/^{13}CO mixtures (obtained for dosing conditions) to zero coverage. Alternatively, $\nu_{CO}(\theta\rightarrow 0)$ could be obtained by extrapolating ν'_{CO} values for pure ^{12}CO layers to zero coverage; however, this procedure has the disadvantage that the ν_{CO}-θ variations are markedly larger due to the substantial coverage dependence of the dipole-coupling component. The resulting $\nu_{CO}(\theta\rightarrow 0)$ values for ^{12}CO are 2018 and 2030 ($\pm$ 2–3) cm^{-1}.

An example of the procedure used to generate $\nu_{CO}(\theta,\text{dl})$, involving a plot of ν_{CO} frequencies at -0.25 V against $\%^{12}$CO, for $\theta = 0.6$ is shown in Fig. 8. Both the higher- and lower-frequency (^{12}CO and ^{13}CO) band partners are plotted. This figure also illustrates that similar $\Delta\nu_D$ values are obtained (30–34 cm^{-1}) for $\theta = 0.6$ from Eq. (1) by utilizing either the ^{12}CO or ^{13}CO band partner.

The resulting plots of $\Delta\nu_D$ (solid traces) and $\Delta\nu_C$ (dashed traces) against θ are shown for adsorption at -0.25 and 0.1 V in Figs. 9(A) and 9(B), respectively. (No individual points are included in these figures, partly because they represent averages of several replicate data sets; however, the uncertainty in both $\Delta\nu_D$ and $\Delta\nu_C$ is about 5 cm^{-1}.) The $\Delta\nu_D$-θ and $\Delta\nu_C$-θ traces marked with arrows denote those obtained under electrooxidative stripping conditions, whereas those without arrows refer to dosing conditions. Inspection of Fig. 9 shows that the coverage-dependent shifts in ν_{CO} frequency obtained under dosing conditions are associated primarily with dynamic dipole–dipole coupling rather than static dipole or "chemical" contributions. For stripping conditions, the latter effect survives virtually intact at least down to $\theta\sim 0.1$. Dosing at -0.25 V yields a relatively smooth, albeit nonlinear, increase in the dipole coupling with coverage [Fig. 9(A)], contrasting the "curvilinear" form of the corresponding plot at 0.1 V [Fig. 9(B)].

One possible complication with this analysis, discussed recently,[13(a)] is that substantial ν_{CO} frequency upshifts with increasing θ may be in part a manifestation of surface defects. This arises chiefly because the CO adsorption on such defects is known to yield smaller ν_{CO} frequencies than for terminal bonding on terrace sites, and the former sites may be filled preferentially at lower coverages. In this event, falsely low $\nu_{CO}(\theta,\text{dl})$ as well as $\nu_{CO}(\theta\rightarrow 0)$ values can be extracted from the data.[13(a)] The influence of this effect certainly could not be eliminated in the present case, even though evidence for the well-ordered nature of Pt(111) surfaces prepared by using the procedure followed here[4] has also been obtained by means of atomic-resolution scanning tunneling microscopy.[29]

Nevertheless, evidence against at least the dominant influence of such defects in the above analysis was gleaned from corresponding ν_{CO} spectra obtained on surfaces con-

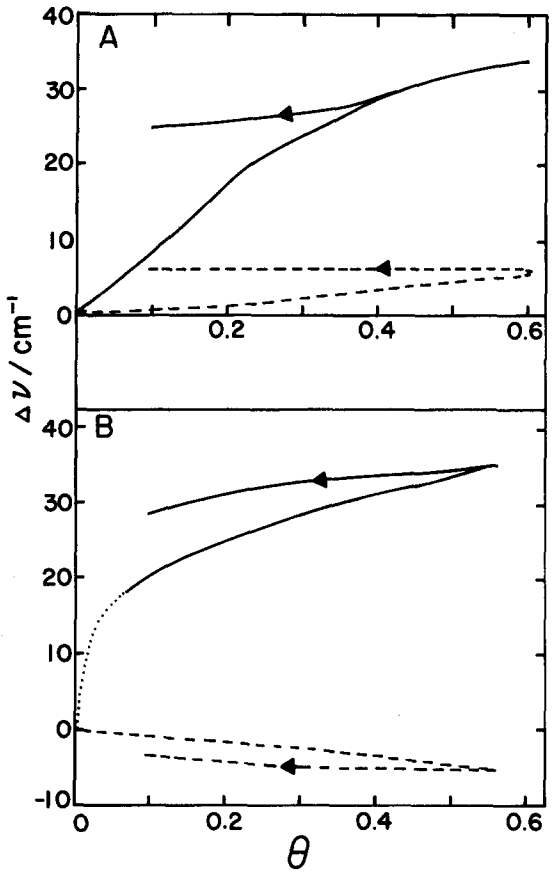

FIG. 9. Plots of coverage-induced ν_{CO} frequency shift due to dynamic dipole–dipole coupling, $\Delta\nu_D$ (solid traces), and to static dipole and chemical interaction effects, $\Delta\nu_C$ (dashed traces) vs coverage θ on Pt(111) at -0.25 V (A) and 0.1 V (B). Traces with and without arrow refer to layers prepared by electrooxidative stripping and dosing methods, respectively. Uncertainties in $\Delta\nu_D$ and $\Delta\nu_C$ values estimated to be about 5 cm^{-1}. Plots extracted from data such as in Figs. 6–8 by using Eqs. (1) and (2). See the text for further details.

taining additional defects caused by sweeping the potential beyond ~ 1.0 V so that "surface disordering" occurs.[3(a),30] This procedure appears to yield randomly distributed monoatomic steps,[30] and results in the disappearance of the voltammetric "butterfly" peaks that are characteristic of a well-ordered Pt(111) electrode surface.[3,4,30] Performing a number (20–30) of such voltammetric cycles (to 1.2 V) in 0.1 M $HClO_4$ indeed yields a platinum surface with infrared spectral as well as electrocatalytic properties[11(a),(c),31] that resemble those of the usual polycrystalline material. Thus CO adsorbed on this surface displays very strong dipole coupling, as evidenced by the presence of a single broad ν_{CO} feature for $^{12}CO/^{13}CO$ mixtures [cf. Ref. 17(a)], as well as noticeably (10–15 cm^{-1}) lower $\nu_{CO}(\theta,\mathrm{dl})$ and $\nu_{CO}(\theta\rightarrow 0)$ values than on ordered Pt(111). Light "surface disordering," caused by 1–2 voltammetric cycles so to produce a relatively low defect concentration yielded little decrease ($\lesssim 5$ cm^{-1}) in either $\nu_{CO}(\theta,\mathrm{dl})$ or $\nu_{CO}(\theta\rightarrow 0)$.

An interesting sidelight to these experiments is that the differences between the ν'_{CO}-θ dependencies noted for stripping and dosage conditions on ordered Pt(111) were found to be diminished substantially by even light surface disordering, markedly greater decreases of ν_{CO} towards lower θ upon electrooxidative stripping generally being obtained than on the ordered surface. A similar behavioral difference between ordered and disordered Pt(111) has been noted previously.[9(a)]

A feature of the present results, already considered, is the significant difference in the coverage dependence of the ν_{CO} spectra formed by dosing at -0.25 V vs 0.1 V. Subtle yet significant structural differences for *saturation* CO coverages formed by adsorption at these two potentials can also be discerned from the infrared spectra. Inspection of Figs. 1 and 3 shows that ν'_{CO} obtained for a saturated CO layer at -0.25 V, 2059 (± 1) cm^{-1}, is very close to that, 2062 cm^{-1}, observed at 0.1 V under these conditions. Given the potential dependence of ν'_{CO}, $d\nu'_{CO}/dE \approx 35$ cm^{-1} V^{-1} for $\theta \approx 0.6$ (*vide infra*),[9(a)] one would expect a larger (10 cm^{-1}) difference between ν'_{CO} at these two potentials. Indeed, a saturated irreversibly adsorbed CO layer formed at 0.1 V and stepped to -0.25 V yielded a lower terminal ν_{CO} frequency, 2048 cm^{-1}, than that observed for dosage at -0.25 V.

These frequency differences might be accounted for by the slightly (~ 0.05) lower saturation coverages formed upon CO dosage at 0.1 V rather -0.25 V, as also noted previously.[9(a)] That this factor provides only an incomplete explanation of the ν_{CO} frequency differences, however, is evident from the plots of ν'_{CO} vs electrode potential assem-

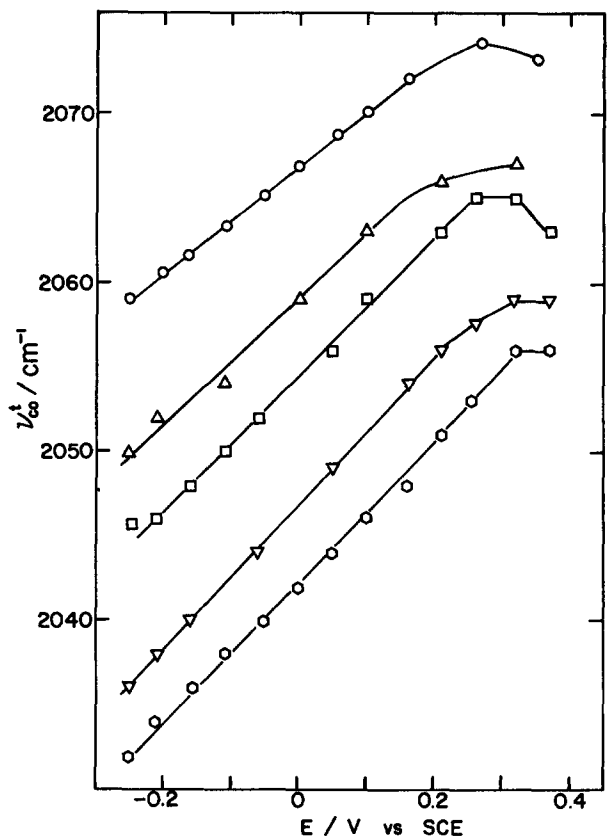

FIG. 10. Peak frequencies of ν_{CO} band vs electrode potential for various ^{12}CO coverages on Pt(111) formed by dosing at -0.25 V. Spectra obtained during 2 mV s^{-1} positive-going potential sweep from -0.25 V. Key to CO coverages: circles, 0.6; upright triangles, 0.45; squares, 0.35; inverted triangles, 0.2; hexagons, 0.12.

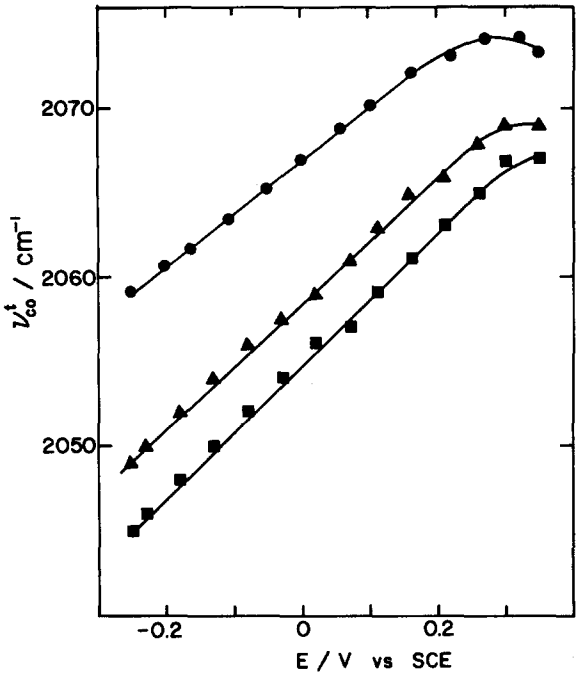

FIG. 11. As for Fig. 10, but for layers formed at -0.25 V by electrooxidative stripping. Key to CO coverages: circles, 0.6; triangles, 0.35; squares, 0.07.

bled in Figs. 10 and 11 for irreversibly adsorbed CO at various θ values formed by dosing and electro-oxidative stripping, respectively. Both groups of ν^t_{CO}-E traces were obtained from sets of interferograms (each 30 scans) taken during slow (2 mV s^{-1}) positive-going potential sweeps from -0.25 V [cf. Ref. 9(a)]. The data in Fig. 11 refer to the same conditions as in Fig. 5 of Ref. 9(a), although the present results extend to lower coverages as a benefit of improved spectral sensitivity. The ν^t_{CO}-E plots are seen to be essentially linear, at least to potentials, $\sim$0.3 V, where electrooxidation commences. The $d\nu^t_{CO}/dE$ slopes increase with decreasing coverage in the range $\theta \approx 0.45$–0.6 (33 cm^{-1} V^{-1} at $\theta = 0.6$), but remain relatively invariant at about 39 and 41–43 cm^{-1} V^{-1} at lower coverages for dosing (Fig. 10) and stripping (Fig. 11) conditions, respectively. The bandwidth is largely independent of potential as well as coverage for layers formed by stripping conditions. For dosed layers, however, the bandwidth diminishes slightly ($\sim$10%–20%) while traversing the potential range -0.25 to 0.2 V at smaller coverages ($\theta \lesssim 0.3$). This effect is qualitatively in accordance with, although smaller than, that expected from Fig. 4. Essentially the same frequencies and band shapes were obtained by examining the ν^t_{CO}-E dependence on time scales down to a few seconds (by employing potential steps) or up to at least 30 min.

Nevertheless, comparison between Figs. 7 and 10 shows that the ν^t_{CO} values obtained at 0.1 V by dosing at -0.25 V and subsequently altering the potential decrease with θ to a greater extent than for layers formed by dosing directly at 0.1 V. In other words, the θ-dependent layer structures formed by CO dosing in the hydrogen region (at -0.25 V), which differ somewhat from those formed in the double-layer region (at 0.1 V), apparently survive when the potential is altered from the former to the latter value. A similar "memory" effect also found upon dosing at 0.1 V and subsequently altering the potential to -0.25 V. This went unnoticed in our earlier study,[9(a)] primarily due to the use of stripping rather than dosing as the usual means of forming intermediate CO coverages.

The potential-dependent behavior of the bridging ν_{CO} feature is comparable in that the ν^b_{CO}-E plots are linear with slopes of 36–38 cm^{-1} V^{-1}, largely coverage independent at least for $\theta \gtrsim 0.3$. The bandshape is not altered perceptibly at a given coverage over the potential range -0.25 to 0.25 V, prior to CO electrooxidation.

The occurrence of coverage-dependent dipole coupling is also anticipated to yield deviations from Beers law whereupon plots of the integrated terminal band absorbance A_i vs θ are convex towards the former axis.[16(a)] We have noted previously,[9(a)] however, that in contrast to Pt(111)/CO in UHV the electrochemical system yields essentially linear A_i-θ plots, at least for $\theta \gtrsim 0.1$. Figure 12 shows A_i-θ plots obtained at -0.25 V for dosing (open circles) as well as for the stripping condition (filled circles) utilized in Ref. 9(a). Indeed, while the latter data are again in good accordance with Beers law, the former exhibit significant positive deviations in a manner qualitatively consistent with coverage-dependent dipole coupling. Corresponding A_i-θ plots obtained by CO dosing as well as stripping at 0.1 V, on the other hand, are essentially linear.

A number of isotopic substitution experiments aimed at probing the extent of exchange between solution and adsorbed CO were also undertaken. Although, as already noted, CO is irreversibly adsorbed on Pt(111) in that the adsorbate remains upon removal of solution CO, the exchange between the solution and adsorbed states was found to be relatively facile in the *presence* of solution CO. Thus addition of solution ^{12}CO following irreversible adsorption of a saturated ^{13}CO layer yields replacement of most ($\sim$80%) of the

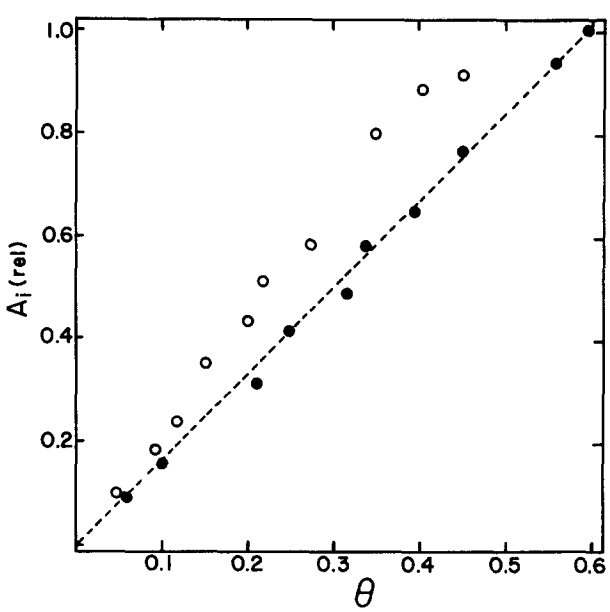

FIG. 12. Integrated absorbance of terminal ν_{CO} band (relative to saturation value) vs CO coverage on Pt(111) at -0.25 V, for adlayers formed by dosing (open circles) and electrooxidative stripping, respectively.

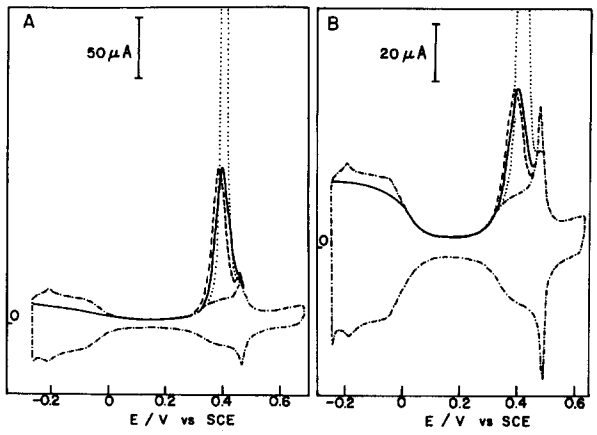

FIG. 13. Anodic-cathodic cyclic voltammograms at 50 mV s^{-1} from -0.25 V for electrooxidation of irreversibly adsorbed CO on Pt(111) in 0.1 M $HClO_4$ for adlayers formed at -0.25 V by prior CO dosing (dashed traces) and electrooxidative stripping (solid traces). CO coverages: (A) $\theta = 0.25$; (B) $\theta \simeq 0.05$. Dashed traces are corresponding voltammograms for a saturated layer ($\theta = 0.6$). Dashed–dotted traces are voltammograms obtained in the absence of adsorbed CO.

latter isotope within ~ 10 min as deduced from the resulting infrared spectra. Experiments were also performed where an irreversibly adsorbed ^{13}CO adlayer was partially removed electro-oxidatively before dosing with low ^{12}CO concentrations. In cases where the adsorbate isotopic substitution was incomplete, the surface infrared spectra exhibited relatively weak dipole coupling, suggesting that adsorption of the fresh CO occurs at microscopically separate patches on the surface. Such isotopic exchange studies can clearly provide much information on the dynamical as well as structural aspects of CO electrochemical adsorption, and will be pursued further elsewhere.

Given the substantial differences in the infrared properties of subsaturated CO layers formed under stripping and dosing conditions, it is of interest to ascertain if there are corresponding differences in the CO electrooxidation kinetics. To this end, Figs. 13(A) and 13(B) contain representative anodic voltammograms at 50 mV s^{-1} for initial CO coverages of 0.25 and 0.05, respectively, formed by dosing (dashed traces) and prior stripping from a saturated adlayer (solid traces) at -0.25 V. The dotted trace refers to electrooxidation of a saturated layer ($\theta = 0.6$), and the dashed–dotted cyclic voltammogram is that obtained for ordered Pt(111) in the absence of CO. Although the shape of the voltammetric waves for CO oxidation are seen to be similar for layers formed by these dosing and stripping conditions,[32] the former are shifted by a small (10–15 mV) yet reproducible amount to lower overpotentials. Comparable results were obtained when using voltammetric sweep rates at least down to 2 mV s^{-1}. No significant voltammetric differences, however, were discerned for such layers formed within the "double-layer" region, i.e., for $E > 0$ V.

DISCUSSION

The present observation of coverage-induced increases in ν_{CO}^{l}, identified primarily with dynamic dipole–dipole coupling, bears a strong resemblance to the behavior of Pt(111)/CO in UHV.[13(a),19,26] The magnitude of the dipole coupling contribution at $\theta \simeq 0.6$, 30–35 cm^{-1}, is slightly larger than that, 20–30 cm^{-1}, derived from recent measurements for the UHV system,[13(a),19] including a detailed study at room temperature.[19] As noted above, it is possible that the relatively large $\Delta\nu_D$ values, and the underlying decreases in ν_{CO}^{l} towards lower coverages, are artifactual in that they arise in part from preferential filling of defect sites. As we have discussed recently,[9(b)] however, besides the obvious differences arising from the presence of solvent and ionic double-layer components in the electrochemical case, the electrostatic surface potentials are markedly different in the electrochemical and UHV systems. Thus, the UHV measurements are necessarily performed at a "potential" (vs vacuum) equal to the metal work function ϕ^M, whereas the electrode potential (vs a reference electrode) E^M is necessarily controlled in the electrochemical system. A general relationship between these quantities is[34]

$$E^M = \phi^M + \delta\chi^M - g^S(\text{dip}) + g_S^M(\text{ion}) - E_T(\text{ref}) , \quad (3)$$

where $\delta\chi^M$ is the change in the "electronic" part of the work function as the metal is contacted with solution, $g^S(\text{dip})$ and $g_S^M(\text{ion})$ are the contributions of solvent dipoles and free charges (ions) to the metal–solution potential drop, and E_T (ref) converts the electrode potential vs the reference electrode to the vacuum scale. This last term has been estimated to be about 4.35 V for the normal hydrogen electrode ($\equiv 4.6$ V for SCE).[35]

Given that ϕ^M is about 5.7 eV for clean Pt(111),[9(b)] and 0.15 V higher for a saturated CO layer,[37] a considerable extrapolation of the electrochemical ν_{CO} frequencies to more positive electrode potentials is required in order to compare these with corresponding UHV values at a common overall interfacial potential, so that[9(b),38]

$$E_0^M = \phi^M - E_T(\text{ref}) . \quad (4)$$

At the potential E_0^M, the solvent dipolar [g^S(dip)] and "free charge" [g_S^M(ion) + $\delta\chi^M$] contributions to E^M nullify each other.[9(b)]

Employing the θ dependent ν_{CO}^{l} and $d\nu_{CO}^{l}/dE$ values from Fig. 10, we estimate a ν_{CO}^{l} value at E_0^M for $\theta = 0.5$ (1.2 V vs SCE), for example, equal to 2105 cm^{-1}. This value is close to (within 10 cm^{-1} of) those reported for the corresponding Pt(111)/CO UHV system at 300 K, 2094[19(a)] and 2099 cm^{-1}.[13(b)] The same extrapolation for the bridging ν_{CO} feature at $\theta = 0.5$, given that $\nu_{CO}^{b} = 1828$ cm^{-1} at -0.25 V [Fig. 5(A)] and $d\nu_{CO}^{b}/dE \simeq 36$ cm^{-1} V^{-1} yields a ν_{CO}^{b} value at E_0^M of 1880 cm^{-1}. This estimate is significantly higher than the corresponding value for the Pt(111)/CO ($\theta = 0.5$) UHV system at 300 K, 1851 cm^{-1}.[13(b)] The singleton ν_{CO}^{l} value in the electrochemical environment (2018 cm^{-1} at -0.25 V) is slightly lower than expected on this basis; assuming that $d\nu_{CO}^{l}/dE \simeq 43$ cm^{-1} V^{-1} yields a ν_{CO}^{l} value at E_0^M (1.1 V vs SCE) of 2076 cm^{-1}, compared with a singleton value of 2082 cm^{-1} in the UHV system.[19(a)] However, such frequency disparities could easily be due to uncertainties in the potential extrapolation.

Consequently, then, the structure of the terminal CO in the electrochemical and UHV environments appears to be

quite similar, although a more specific influence of the double layer is probably being felt within the bridging adsorption geometry. A further indication of the significant role played by the electrochemical environment upon the adlayer structure can be gleaned from the coverage-dependent band intensities. The ~3.5-fold smaller integrated absorbance of the bridging vs terminal CO bands for dosed layers at $\theta \approx 0.5$ (Fig. 5) is closely similar to the corresponding intensity ratio of the Pt(111)/CO ($\theta = 0.5$) UHV system at 300 K.[13(b)] The latter is consistent with a $c(4\times2)$ adlayer structure featuring equal occupancy of on-top and twofold bridging sites, given that the absorptivity of the bridging ν_{CO} band, ϵ_b, is about 2.5-fold smaller than for the terminal band, ϵ_t[13(b)] [cf. behavior on Rh(111) [12(a)]]. The virtual disappearance of the bridging feature in the presence of solution CO (i.e., for a compressed layer) also mirrors the behavior in UHV.[13(a),15] However, the progressive increase in the bridging/terminal integrated intensity ratio $A(b/t)$ with decreasing θ for dosed layers (Fig. 5) contrasts sharply with the behavior of the UHV system: the latter exhibits $A(b/t)$ ratios that diminish continuously with decreasing coverage for $\theta < 0.5$.[13,15] This implies that the site occupancy in the electrochemical environment, unlike the UHV system, shifts increasingly in favor of the bridging form at smaller coverages. Note, however, that this conclusion only applies to dosed layers; for electro-oxidatively stripped layers, $A(b/t)$ and hence the site occupancy do not alter markedly as θ diminishes. This issue will be returned to below.

A striking feature of the present results is the marked difference in the form of the $\Delta\nu_D$- and ν^t_{CO}-coverage dependence depending upon whether CO dosing or electrooxidative stripping conditions are employed, and if coadsorbed hydrogen or water is present. The relatively small changes in both $\Delta\nu_D$ and ν^t_{CO}, and also $A(b/t)$, as θ decreases upon electro-oxidative stripping (Figs. 6, 7, and 9) show that the average CO environment changes little under these conditions. Such behavior is indicative of the formation of CO patches or "islands," in which the initially saturated CO layer is oxidized by a nucleation-growth mechanism involving reaction at island edges with water or hydroxyl radicals. Although such an electrooxidation mechanism has been considered previously,[39,40] the present results provide strikingly direct evidence for its occurrence.

It is possible in principle to estimate rough island dimensions from coverage-dependent dipole-coupling data.[16(a),16(c),19] A convenient means of inspecting the data for this purpose, employed recently for the Pt(111)/CO UHV system,[19] is in the form of plots of $[\nu^2_{CO}(\theta) - \nu^2_{CO}(\theta,\mathrm{dl})]$ vs θ. As indicated in Ref. 19(b), such plots are expected to be roughly linear with small intercepts if the surface is filled with CO "monomers" or small ($n \sim 4$) CO clusters in random arrays. If sufficient clustering occurs so to form larger islands (say $n > 50$) over substantial coverage ranges, however, these plots will be highly nonlinear and/or exhibit substantial y intercepts, reflecting the relative invariance of the CO environment as θ is lowered.

Figure 14 is such a $[\nu^2_{CO}(\theta) - \nu^2_{CO}(\theta,\mathrm{dl})]$–$\theta$ plot for the electrochemical Pt(111)/CO system at −0.25 V for dosing and stripping conditions, the latter trace again being

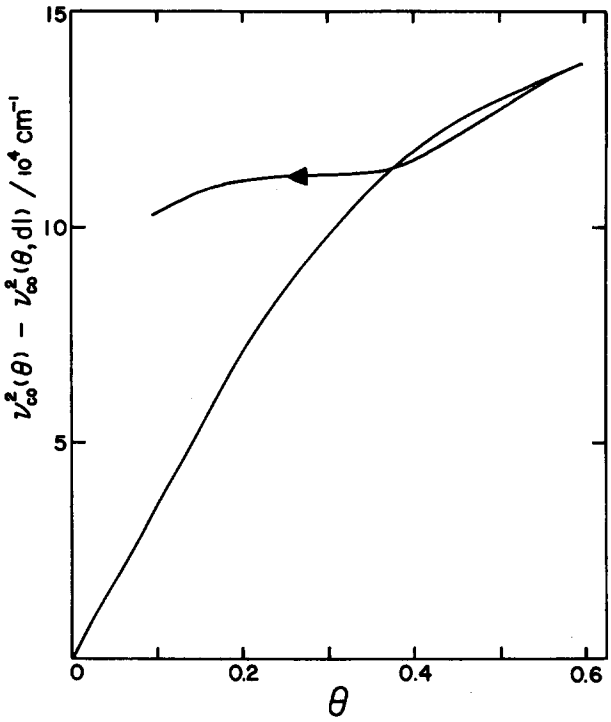

FIG. 14. Plot of $[\nu^2_{CO}(\theta) - \nu^2_{CO}(\theta,\mathrm{dl})]$, where $\nu_{CO}(\theta)$ is the pure ^{12}CO frequency and $\nu_{CO}(\theta,d1)$ is this frequency at the same coverage but in the dilution limit with ^{13}CO, vs the CO coverage θ for adsorption at −0.25 V. Traces with and without arrow refer to adlayers formed by electro-oxidative stripping and CO dosing, respectively. See the text for further details.

denoted by an arrow (cf. Fig. 8). For electrooxidative stripping conditions, the substantial y intercept in Fig. 14 is indicative of extensive CO island formation, as already inferred from Figs. 7 and 9(A). Similarly shaped curves are obtained for dosing as well as stripping conditions at 0.1 V, again signaling the occurrence of extensive island formation in the presence of water coadsorption. The formation of moderate or large CO islands ($n \gtrsim 20$) is also predicted to yield ν_{CO} bands having a significant "tail" on the low-frequency side, resulting from the environmental differences experienced by CO situated towards the center and periphery of the islands.[16(a)] Such band shapes are indeed observed, more noticeably for CO stripping conditions [Figs. 1(A) and 1(B)], providing a further indication of extensive island formation under these conditions. The corresponding trace obtained for direct dosing conditions is markedly more linear (Fig. 14), suggesting that CO island formation is less extensive, or at least that the patches have a coverage-dependent size. While this conclusion is probably qualitatively sound, a complication is that under dosing conditions the coverage of the terminal CO form θ_t required for this analysis,[41] is not strictly proportional to the *overall* coverage plotted in Fig. 14. From Fig. 5 and the above discussion, θ_t falls rapidly with decreasing θ, reflecting the relatively greater occupancy of the bridging rather than terminal adsorption sites. Consequently, then, plotting $[\nu^2_{CO}(\theta) - \nu^2_{CO}(\theta,\mathrm{dl})]$ vs θ_t rather than θ for dosed layers (either at −0.25 or 0.1 V) will yield more nonlinear plots with larger y intercepts, indicative of more extensive island formation than is apparent from Fig. 14.

The corresponding analysis of the Pt(111)/CO UHV system at 300 K yields roughly linear $[\nu^2_{CO}(\theta) - \nu^2_{CO}(\theta,dl)]$-$\theta$ plots with zero intercept, with the inference that little or no CO island formation occurs under these conditions.[19] [This conclusion differs from that of an earlier IRRAS study for the Pt(111)/CO UHV system.[26]] It is therefore of interest to speculate on the likely reasons for this marked behavioral difference between the electrochemical and UHV systems.

The origin of these differences can be traced in part to the effect of coadsorbed water and/or hydrogen in the electrochemical environment. Evidence of the formation of separate islands of coadsorbed water and CO on Pt(111) in UHV has been obtained from thermal desorption and EELS data.[42] Thus net repulsive CO–water interactions are implicated from the observed depression of the water desorption temperature in the presence of CO, and the vibrational features of adsorbed water are unaffected by CO coadsorption. Water coadsorption yields a downshift of ν'_{CO} to $\sim$2080 cm^{-1},[42,43] closer to the present electrochemical ν_{CO} frequencies; moreover, a bridging ν_{CO} band at $\sim$1830 cm^{-1} appears at CO coverages, $\theta \lesssim 0.2$, where it is entirely absent for the anhydrous system.[42] The last observation, in particular, suggests that the *local* coverage within the CO islands is relatively high, such that adsorbate structures akin to the $c(4\times2)$ adlattice, featuring both bridging and terminal CO, are formed.[42] The presence of a substantial fraction of bridging CO even at similarly low dosed coverages in the electrochemical environment (Fig. 5) can therefore also be attributed in part to the formation of islands, within which the CO is present at high local coverage.

A recent IRRAS study of coadsorbed H and CO on Pt(111) in UHV by Hoge *et al.*[44] together with information from thermal energy atom scattering[45] shows convincingly that aggregation into CO islands occurs, at least in the temperature range 100–180 K. (The upper temperature limit is determined by the onset of H desorption.) Similarly to water coadsorption, the presence of coadsorbed hydrogen in the Pt(111)/CO UHV system also produces bridging CO at low average coverages, $\theta < 0.25$.[44] Again, this is consistent with CO island formation, and can rationalize the qualitatively similar observation for the electrochemical system with coadsorbed hydrogen [Fig. 5(A)]. In the presence of substantial coadsorbed hydrogen, Hoge *et al.* observe that the terminal ν_{CO} band shifts to lower frequencies and broadens to a markedly greater extent with decreasing CO coverage than is observed in the absence of hydrogen.[13(a)] They attribute this and related behavior to a θ-dependent distribution of island sizes and/or local CO packing densities.[44] This behavior is strongly reminiscent of that observed in the electrochemical environment with coadsorbed hydrogen, both with regard to the ν'_{CO}-θ [Figs. 1(B), 6] and $\Delta\nu_{1/2}$-θ [Figs. 1(B), 4] behavior. Although the temperature of the latter environment is necessarily higher than can be attained in the corresponding UHV system, it is tempting to suggest that a qualitatively similar θ-dependent distribution of CO aggregates are also present in the electrochemical system.

A caveat should be added, however: although the large ($\sim$30 cm^{-1}) ν'_{CO} decreases observed over the CO coverage range $0.6 > \theta > 0.05$ in the Pt(111)/CO,H UHV system apparently match those in the electrochemical case (Fig. 5), the former system should be characterized by a significant ($\sim$0.2–0.3 V) diminution in work function as θ is decreased. [Adsorbed H engenders such ϕ^M decreases on Pt(111),[46] whereas CO does not.[37]] Unlike the UHV system, however, the electrode surface is held at a constant potential, so that this work function alteration in the electrochemical case will automatically be compensated by a corresponding change in the free-charge component of the double-layer potential [g^M_S (ion) in Eq. (3)]. In view of the above discussion, then, the presence of this latter component in the electrochemical case may offset the decreases in ν'_{CO} due to coadsorbed H as seen in the UHV system.

Recent LEED measurements for CO layers on Pt(111), formed by CO dosing (as here, in 0.1 M $HClO_4$ at $\sim$0.1 V vs SCE) and subsequently transferrred to UHV, are also strongly suggestive of CO island formation.[47] Thus a $c(\sqrt{3}\times5)$rect LEED structure is obtained over a range of intermediate coverages, indicating the presence of CO in patches of locally high packing density, whereas a distinct $(\sqrt{3}\times3)$rect structure was obtained at saturation coverage.[47] These "*ex situ*" LEED observations are indeed consistent withthe corresponding *in situ* IRRAS results (Fig. 7) in that the ν'_{CO} values initially decrease for coverages just below saturation, then alter little over the range $0.3 \lesssim \theta \lesssim 0.5$, even for CO dosing conditions. As outlined in Ref. 16(c), such a ν'_{CO}-θ "arrest region" is suggestive of the formation of a CO domain structure distinct from that obtained at saturation.

Having highlighted the role of coadsorbed water and hydrogen, it is necessary to point out that these factors cannot account entirely for the relative importance of the bridging adsorption geometry at low dosed coverages in the electrochemical system (Fig. 5). Thus merely compressing the CO into domains of higher local coverage should simply yield band intensity ratios $A(b/t)$ that mimic those found at high θ; instead, however, larger $A(b/t)$ values are obtained at lower average coverages. This suggests that another factor is additionally responsible for the differences in site occupancy between the electrochemical and UHV systems. A recent theoretical study of the Pt(111)/CO system[48] indicates that the imposition of negative potential (and hence charge) increasingly favors CO adsorption at bridging rather than terminal sites, due to the increased extent of $d\pi$(Pt)-$2\pi^*$(CO) back bonding under these conditions. The observed greater propensity of bridging adsorption in the electrochemical vs the UHV environments at low CO coverages can therefore be understood on this basis, given the more negative surface potentials that typify the former system (*vide supra*). Most likely, the close similarity in the site occupancies seen in these two environments at higher coverages result from adlayer packing considerations.

The significant (up to $\sim$25%) increase in the $d\nu'_{CO}/dE$ slope observed as θ decreases, especially following dosing at -0.25 V (Fig. 9), provides another manifestation of the coverage-dependent alterations in the adlayer structure. Most simply, this effect may be attributed to alterations in the local surface environment, from primarily adsorbed CO to coadsorbed H/H_2O, as θ is decreased. Interestingly, how-

ever, evidence of significant tilting of adsorbed CO molecules on Pt(111) away from the surface normal at the highest CO coverages ($\theta \gtrsim 0.6$) has recently been obtained in UHV by means of ESDIAD.[49] Such tilting would be expected to lead to smaller $d\nu_{CO}^{t}/dE$ slopes, at least on the basis of "Stark tuning" arguments,[48,50] since the effective inner-layer field strength experienced by the CO molecules would be correspondingly diminished. The observation of such smaller $d\nu_{CO}^{t}/dE$ slopes only for CO coverages close to saturation (Figs. 10 and 11) provides some support to this interpretation.

The present finding that smaller and more coverage-dependent CO island sizes result from CO dosing in the electrochemical hydrogen region also provides a rationale of the more facile CO electrooxidation kinetics observed for such adlayers vs those formed by prior stripping from a saturated CO layer (Fig. 12). Given that CO electrooxidation is perceived to occur at the island edges (*vide supra*),[39,40] the presence of a greater number of smaller islands for a given coverage θ will provide a greater fraction of CO located at such reactive sites, and hence should yield a greater electrooxidation rate at a given overpotential, as is observed. We have also observed qualitatively similar, although rather more pronounced, effects upon both the ν_{CO} spectra and the CO electrooxidation kinetics for CO adlayers on Pt(110) and (100) surfaces formed by dosing vs prior partial stripping. These results are reported elsewhere [9(c),9(d)]

Even though there are significant uncertainties in the interpretation of the present findings as regards the possible role of surface defects, we believe that they demonstrate some previously unexploited virtues of IRRAS for gaining detailed *in situ* structural information for molecular adsorbates at monocrystalline metal–solution interfaces. Especially given the burgeoning usage of IRRAS as a structural and dynamical probe of the closely related UHV systems, application of this technique for gaining corresponding insight for structurally well-defined electrochemical surfaces seems destined to expand rapidly in the near future.

ACKNOWLEDGMENTS

Professor Andrzej Wieckowski kindly supplied Ref. 47 in advance of publication. This work is supported by the National Science Foundation.

[1]For recent reviews, see J. T. Yates, Jr. and T. E. Madey, *Vibrational Spectroscopy of Molecules on Surfaces* (Plenum, New York, 1987).

[2]For example, see S. Pons, J. K. Foley, J. Russell, and M. Severson, in *Modern Aspects of Electrochemistry*, Vol. 17, edited by J. O.'M. Bockris, B. E. Conway, and R. E. White (Plenum, New York, 1986), Chap. 3.

[3](a) J. Clavilier, R. Faure, G. Guinet, and R. Durand, J. Electroanal. Chem. **107**, 205 (1980); (b) J. Clavilier, J. Electroanal. Chem. **107**, 211 (1980); (c) J. Clavilier, ACS Sym. Ser. **378**, 202 (1988).

[4](a) D. Zurawski, L. Rice, M. Hourani, and A. Wieckowski, J. Electroanal. Chem. **230**, 221 (1987); (b) M. Hourani and A. Wieckowski, *ibid.* **227**, 259 (1987).

[5]For a review, see R. Parsons and T. Vandernoot, J. Electroanal. Chem. **257**, 9 (1988).

[6]L. -W. H. Leung and M. J. Weaver, Langmuir **6**, 323 (1990).

[7](a) P. Kitamura, M. Takahashi, and M. Ito, J. Phys. Chem. **92**, 3320 (1988); (b) F. Kitamura, M. Takeda, M. Takahashi, and M. Ito, Chem. Phys. Lett. **142**, 318 (1987).

[8]N. Furuya, S. Motoo, and K. Kunimatsu, J. Electroanal. Chem. **239**, 347 (1988).

[9](a) L.-W. H. Leung, A. Wieckowski, and M. J. Weaver, J. Phys. Chem. **92**, 6985 (1988); (b) S.-C. Chang, L.-W. H. Leung, and M. J. Weaver, J. Phys. Chem. **93**, 5341 (1989); (c) S.-C. Chang and M. J. Weaver, Surf. Sci. (in press); (d) S.-C. Chang and M. J. Weaver, J. Phys. Chem. (in press).

[10](a) S. Juanto, B. Beden, F. Hahn, J.-M. Leger, and C. Lamy, J. Electroanal. Chem. **237**, 119 (1987); (b) B. Beden, S. Juanto, J. M. Leger, and C. Lamy, *ibid.* **238**, 323 (1987); (c) S. C. Sun, J. Clavilier, and A. Bewick, *ibid.* **240**, 147 (1988).

[11](a) L.-W. H. Leung, S.-C. Chang, and M. J. Weaver, J. Electroanal. Chem. **266**, 317 (1988); (b) L.-W. H. Leung and M. J. Weaver, J. Phys. Chem. **93**, 7218 (1989); (c) S.-C. Chang, L.-W. H. Leung, and M. J. Weaver, J. Phys. Chem. (in press).

[12](a) L.-W. H. Leung, S.-C. Chang, and M. J. Weaver, J. Chem. Phys. **90**, 7426 (1989); (b) S.-C. Chang and M. J. Weaver, J. Electroanal. Chem. (in press).

[13](a) M. Tüshaus, E. Schweizer, P. Hollins, and A. M. Bradshaw, J. Electron Spec. Related Phenon **44**, 305 (1987); (b) E. Schweizer, B. N. J. Persson, M. Tüshaus, D. Hoge, and A. M. Bradshaw, Surf. Sci. **213**, 49 (1989), and previous references listed therein.

[14](a) J. P. Biberian and M. A. Van Hove, Surf. Sci. **138**, 961 (1984); (b) D. F. Ogletree, M. A. Van Hove, and G. A. Somorjai, Surf. Sci. **173**, 351 (1986).

[15]B. E. Hayden and A. B. Bradshaw, Surf. Sci. **125**, 787 (1983).

[16]For explanative discussions, see (a) P. Hollins and J. Pritchard, Prog. Surf. Sci. **19**, 275 (1985); (b) B. E. Hayden, in *Vibrational Spectroscopy of Molecules on Surfaces*, edited by J. T. Yates, Jr. and T. E. Madey (Plenum, New York, 1987), Chap. 7; (c) F. M. Hoffman, Surf. Sci. Rep. **3**, 107 (1983).

[17](a) M. W. Severson, A. Russell, D. Campbell, and J. W. Russell, Langmuir **3**, 202 (1987); (b) A. Bewick, M. Razaq, and J. W. Russell, J. Electroanal. Chem. **256**, 165 (1988).

[18]P. Gao and M. J. Weaver, J. Phys. Chem. **93**, 6205 (1989).

[19](a) C. W. Olsen and R. I. Masel, Surf. Sci. **201**, 444 (1988); (b) C. W. Olsen and R. I. Masel, J. Vac. Sci. Technol. A **6**, 792 (1988).

[20]D. S. Corrigan and M. J. Weaver, J. Phys. Chem. **90**, 5300 (1986).

[21](a) D. S. Corrigan, L.-W. H. Leung, and M. J. Weaver, Anal. Chem. **59**, 2252 (1987); (b) D. S. Corrigan and M. J. Weaver, J. Electroanal. Chem. **241**, 143 (1988).

[22]For example, H. Seki, K. Kunimatsu, and W. G. Golden, Appl. Spect. **39**, 437 (1985).

[23]A. M. Bradshaw and E. Schweizer, in *Advances in Spectroscopy*, Spectroscopy of Surfaces, Vol. 16, edited by R. J. H. Clark and R. E. Hester (Wiley, New York, 1988), Chap. 8.

[24]P. R. Norton, J. A. Davies, and T. E. Jackman, Surf. Sci. **122**, L593 (1982).

[25]Note that this tactic exploits the fact that virtually all the solution CO_2 remains trapped within the thin-layer cavity on the time scale ($<$ few minutes) of these measurements (Ref. 21).

[26]A. Crossley and D. A. King, Surf. Sci. **95**, 131 (1980).

[27]The band absorptivity ϵ will be slightly smaller for the heavier isotope in proportion to the square of the isotopic frequency ratio (Ref. 28). For the present case, $\epsilon(^{13}CO_2)/\epsilon(^{12}CO_2) = (2275)^2/(2343)^2 = 0.94$.

[28]S. Pinchos and I. Laulicht, *Infrared Spectra of Labelled Compounds* (Academic, London, 1971), Chap. 9.

[29]B. C. Schardt, S.-L. Yau, and F. Rinaldi, Science **243**, 1050 (1989).

[30]F. T. Wagner and P. N. Ross, Jr., J. Electroanal. Chem. **250**, 301 (1988).

[31]S.-C. Chang and M. J. Weaver (to be published).

[32]Voltammograms for CO electrooxidation on Pt(111), particularly at higher intermediate coverages, were often found to display a pair of peaks, or a shoulder preceding the main peak (cf. Ref. 33). Such behavior was especially prevalent when using higher perchloric acid concentrations (>0.5 M $HClO_4$), for solutions containing traces ($\gtrsim 10^{-5}$ M) of CO, or for surfaces left for substantial time periods ($\gtrsim 3$ h) following the annealing pretreatment procedure. The phenomenon was also more pronounced for irreversibly adsorbed layers formed by partial stripping rather than by solution CO dosing. For relatively freshly annealed Pt(111) surfaces in 0.1 M $HClO_4$, purged thoroughly to remove solution CO, however, such peak splitting was typically not observed in the present study.

[33]L. Palaikis, D. Zurawski, M. Hourani, and A. Wieckowski, Surf. Sci. **199**, 183 (1988).

[34]S. Trasatti, J. Electroanal. Chem. **150**, 1 (1983).

[35]The quantity E_T(ref) is equal to $(E_k - \chi^s)$, where E_k is the so-called "absolute potential" of the reference electrode, and χ^s is the surface potential of the solution-air interface. Given that E_k for the normal hydrogen electrode (NHE) is about 4.5 V (within 0.1–0.2 V), (Ref. 34) and $\chi^s \approx 0.13$ V, (Ref. 36) then E_T(ref) ~ 4.35 V for NHE.
[36]S. Trasatti, J. Chem. Soc. Faraday Trans. 1, **70**, 1752 (1974).
[37]P. R. Norton, J. W. Goodale, and E. B. Selkirk, Surf. Sci. **83**, 189 (1979).
[38]The analysis employed here differs slightly from that in Ref. 9(b), in that the latter used the "absolute reference electrode potential" E_k (≈ 4.5 V vs NHE) in place of E_T(ref) [Eqs. (3),(4)]. In addition, the electrochemical ν'_{CO} data used in Ref. 9(b) were those reported earlier, [Ref. 9(a)] which refer to "stripping" rather than "dosing" conditions. Data for the latter condition (Fig. 10) are utilized here.
[39]S. Gilman, J. Phys. Chem. **67**, 78 (1963); **68**, 70 (1964).
[40]For a recent discussion, see B. Love, and J. Lipkowski, ACS Symp. Ser. **378**, 484 (1988).
[41]This is because only the terminally bound CO molecules will contribute to the dynamic dipole–dipole coupling involving this adsorption geometry, since the ν_{CO} frequency of the bridging CO is substantially smaller [for relevant discussions, see Refs. 13(a) and 16(a)].
[42]F. T. Wagner, T. E. Moylan, and S. J. Schmieg, Surf. Sci. **195**, 403 (1988).
[43]W. J. Tornquist and G. L. Griffin, J. Vac. Sci. Technol. A **4**, 1437 (1986).
[44]D. Hoge, M. Tüshaus, and A. M. Bradshaw, Surf. Sci. **207**, L935 (1988).
[45](a) S. L. Bernasek, K. Leuz, B. Poelsema, and G. Comsa, Surf. Sci. **183**, L319 (1987); (b) K. Lenz, B. Poelsema, S. L. Bernasek, and G. Comsa, *ibid.* **189/190**, 431 (1987).
[46]K. Christmann and G. Ertl, Surf. Sci. **60**, 365 (1976).
[47]D. Zurawski, M. Wasberg, and A. Wieckowski, J. Phys. Chem. (in press).
[48]S. P. Mehandru and A. B. Anderson, J. Phys. Chem. **93**, 2044 (1989).
[49]M. Kiskinova, A. Szabó, and J. T. Yates, Jr., Surf. Sci. **205**, 215 (1988).
[50]D. K. Lambert, J. Chem. Phys. **89**, 3847 (1988), and references cited therein.